Available online at www.sciencedirect.com
ScienceDirect
International Journal of Heat and Mass Transfer 51 (2008) 4047–4054
International Journal of HEAT and MASS TRANSFER
www.elsevier.com/locate/ijhmt

Experimental investigation of capillary-assisted evaporation on the outside surface of horizontal tubes

Z.Z. Xia *, G.Z. Yang, R.Z. Wang

Institute of Refrigeration and Cryogenics, Shanghai Jiao Tong University, Shanghai 200240, PR China

Received 14 March 2007; received in revised form 9 July 2007
Available online 20 February 2008

Abstract

Capillary-assisted evaporation is a typical heat transfer method in heat pipes which is characterized by high evaporation coefficient due to extremely thin liquid film. This paper introduces such a micro-scale heat transfer method into normal-scale applications. A series of enhanced heat transfer tubes with circumferential rectangular micro-grooves on the outside surfaces have been experimentally investigated. The aim is to investigate the influence of the tubes' geometries and operating parameters on the evaporation heat transfer coefficients. In the experiment, the tested tubes are hold horizontally and the bottom surfaces are immersed into a pool of liquid. The heat is added to the thin liquid film inside the micro-grooves through the heating fluid flowing inside the tubes. The factors influencing the capillary-assisted evaporation performance, such as the immersion depth, evaporation pressure, superheating degree, etc. are considered. The experimental results have indicated that there is a positive correlation between the evaporation heat transfer coefficient and evaporation pressure, and negative for the superheating and immersion depth. For water, under the evaporation saturated temperature of 5.0 ± 0.1 °C, the superheating of 4.0 ± 0.1 °C and the dimensionless liquid level of 1/2, the film side evaporation heat transfer coefficients are 3100–3500 W/m^2 K, which are equivalent to those of the falling film evaporator in LiBr–water absorption machine (2800–4500 W/m^2 K [Y.Q. Dai, Y.Q. Zheng, LiBr–water Absorption Machine, first ed., Chinese National Defence Industry Press, Beijing, China, 1980.]).
© 2008 Elsevier Ltd. All rights reserved.

Keywords: Capillary-assisted; Enhanced tube; Film evaporation; Experimental investigation

1. Introduction

Capillary-assisted evaporation is gaining more and more attentions in recent years for its high heat transfer coefficient benefited from the extremely thin evaporating liquid film. The previous researches concerning the capillary-assisted evaporation can be divided into two branches: one is the fundamental researches on its heat and mass transfer mechanism, and most of them are based on the physical model of an extended meniscus [2–13]; the other is the application researches of such evaporation method, and, usually, the tubes with outside or inside enhanced surfaces are the research objects [14–16].

Before the occurrence of micro-scale manufacture techniques, such as electrical discharge machining (EDM) of metals and chemical etching of silicon, the micro passages for liquid flow are usually supplied by porous materials, such as a sintered metal, a felt metal or a layered screen [17]. For such cases, the liquid flow resistance is very high which has led to a narrow application of capillary-assisted evaporation. The micro-scale manufacture techniques has made it easier to machine regular micro channels with triangular, trapezoidal, sinusoidal or rectangular cross-sections which can provide a better balance between capillary suction and frictional flow resistance.

In previous researches, the micro-grooves with triangular cross-sections have obtained most attentions [2–6] for two advantages: one is easy groove machining, the other is such grooves can avoid the appearance of "dead zone"

* Corresponding author. Tel./fax: +86 21 34206548.
E-mail address: xzz@sjtu.edu.cn (Z.Z. Xia).

0017-9310/$ - see front matter © 2008 Elsevier Ltd. All rights reserved.
doi:10.1016/j.ijheatmasstransfer.2007.11.042

Nomenclature

A	area, m^2
$\overline{A}$	disjoining constant, J
a, b	coefficients in Eq. (2)
Bo	bond number
D	groove depth, m
D_1, D_2	diameters, m
d	the inner diameter of the glass tube liquid level meter, m
g	gravity acceleration, m s^{-2}
H	height, m
h	heat transfer coefficient, W m^{-2} K^{-1}
h_{fg}	evaporation latent heat, J kg^{-1} K^{-1}
K	curvature, m^{-1}
L	tube length, m
$\dot{m}$	evaporation mass flow rate, kg m^{-2} s^{-1}
P	groove pinch, m
p	pressure, Pa
Q	heat flux, W
q	heat flux rate, W m^{-2}
r	the radius of curvature, m
s	circumferential direction
T	temperature, °C
t	time, s
W	groove width, m
x, y	coordinates

Greeks symbols

Δ	difference and error
$\delta, \delta_0, \delta_1$	liquid film thickness, m
ϕ	circumferential angle
Γ_2	mass flow rate, kg m^{-2} s^{-1}
γ	dimensionless liquid level
Λ	shape parameter (D/W)
λ	heat conductivity, W m^{-1} K^{-1}
σ	surface tension, N m^{-1}

Subscripts

e	evaporation
l	liquid
v	vapor
w	wall

and "separated corner flow", which are possibly encountered for the grooves with rectangular cross-sections. However, comparing to triangular micro-grooves, rectangular micro-grooves have more flow cross-sectional area and, thus, less flow resistance and more axial mass flux under the same driving force. Also, the "dead zone" and "separated corner flow" can be avoided by proper structure design. Therefore, the mass and heat transfer thermo-kinetics in rectangular micro-grooves have become to be the focuses of many researches recently [12,13].

The research in this paper is motivated initially by the problems encountered in low pressure evaporators, such as water evaporator, methanol evaporator, etc. For low pressure evaporators, falling film evaporation prevails to avoid the influence of liquid depth on the evaporation saturated temperature. In falling film evaporation, a circulating closed pump and liquid spray equipment are needed, which has caused two problems: one is the system becomes more complex, the other is the non-uniform liquid distribution on the outside surfaces of heat transfer tubes. However, capillary-assisted evaporation can solve the two problems perfectly and thus it has the potential to be a more suitable heat transfer method for low pressure and compact evaporator.

In this paper, a single tube capillary-assisted evaporator is designed to investigate the heat and mass transfer in the capillary-assisted evaporation. Four types of tubes with different micro-groove geometries have been tested and different factors which influence the capillary-assisted evaporation performance have been considered in the experiment.

2. A brief description of capillary-assisted evaporation and capillary-assisted evaporator

The schematic diagram of capillary-assisted evaporation principle is shown in Fig. 1. A heat transfer tube with outside circumferential micro-grooves is immersed into a pool of liquid. By capillary suction, the liquid will flow upwards along the micro-grooves and thus the most outside surface of the tube will be covered by a thin liquid film. Heated by the hot fluid flowing inside the tube, the liquid film outside will evaporate. The schematic diagram of a capillary-assisted water evaporator developed by the research group in Shanghai Jiao Tong University of China is given by Fig. 2. This capillary-assisted water evaporator is applied to a silica gel–water adsorption chiller, and the high heat transfer efficiency has made the evaporator very compact

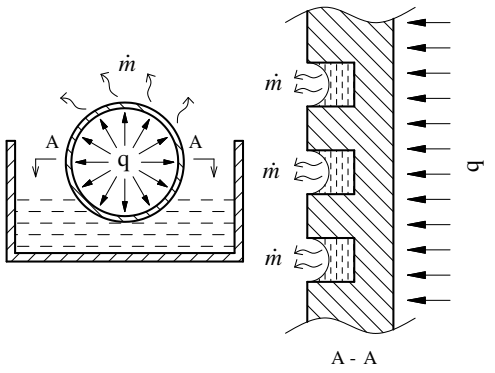

Fig. 1. Capillary-assisted evaporation principle.

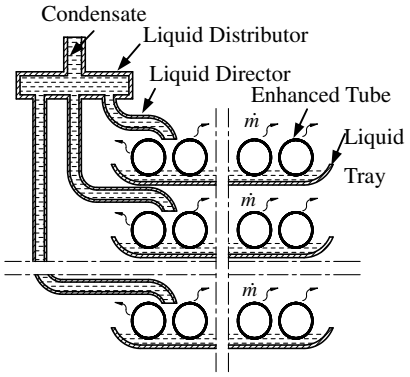

Fig. 2. The schematic of a capillary-assisted evaporator [14].

that is a compensation of the bigger chiller size caused by the low energy density inside adsorption beds [18].

3. Theoretical analysis of capillary-assisted evaporation

The capillary-assisted flow and evaporation inside a circumferential rectangular micro-groove is sketched in Fig. 3. Due to surface tension, the liquid–vapor interface inside the micro-groove is curved that leads to a pressure jump across the interface. This pressure jump can be calculated by the augmented Young–Laplace equation [19]

$$p_v - p_l = \sigma K + \frac{\overline{A}}{\delta^3}, \tag{1}$$

where σ is liquid surface tension, K is liquid–vapor interface curvature, and the term σK represents the pressure jump caused by surface tension. The symbol $\overline{A}$ is disjoining constant (a positive value here), δ is liquid film thickness, and the term $\overline{A}/\delta^3$ represents the pressure jump caused by disjoining pressure. For the micro-groove of sub-millimeter size, the Bond number $Bo = \rho g W^2/\sigma$ is very small, so the liquid–vapor interface curvature K can be treated as constant for any groove axial cross-section. The curvature K, usually assumed zero at the groove's liquid inlet, increases gradually along the groove's axial direction, which produces a pressure gradient to drive the liquid to flow upwards. Such meniscus deformation is shown in Fig. 3a. An axial cross-section of the rectangular groove is shown in Fig. 3b and a local magnifying figure is shown in Fig. 3c. As the liquid moves towards the apex of the groove (see Fig. 3c), the liquid film becomes thinner and thinner, and the term $\overline{A}/\delta^3$ in Eq. (1), i.e., the disjoining pressure, increases quickly. The gradual increase of disjoining pressure produces a decrease in liquid pressure which drives the liquid film to move to the groove's apex. The extended meniscus in Fig. 3b can be divided into three regions: the intrinsic meniscus region, the evaporating thin film region, and the non-evaporating adsorbed film region which are marked as III, II, and I respectively, in Fig. 3c. For the intrinsic meniscus III, the liquid–vapor interface curvature K is constant for any groove's axial cross-section and the disjoining pressure term $\overline{A}/\delta^3$ can be neglected for thicker liquid film. The evaporating thin film region II and the region III are separated at the point where the liquid film thickness gradient $d\delta/dz$ equals to the tangential value of the dynamic contact angle θ. For the evaporating thin film region II, the most amount of heat transferred concentrates in the area close to the non-evaporating adsorbed film region where the liquid film is extremely thin and the thermal resistance is very low. Moreover, the curvature K in this area is so small that the surface tension can be neglected compared to disjoining force. Therefore, the evaporation in the region II is dominated by disjoining force. In the region I, the liquid film is too thin and adsorbed by the solid wall which hinders the liquid from evaporating. Therefore, though the liquid in this region is superheated, no evaporating occurs and the heat flux here is zero. The regions I and II are separated at the groove apex where the liquid film thickness gradient $d\delta/dz$ reduces to zero and z-coordinate is zero. Due to the high axial flow resistance in the evaporating thin film region and the non-evaporating adsorbed film region, majority of the axial flow will be confined to the intrinsic meniscus region and the area under this region inside the groove.

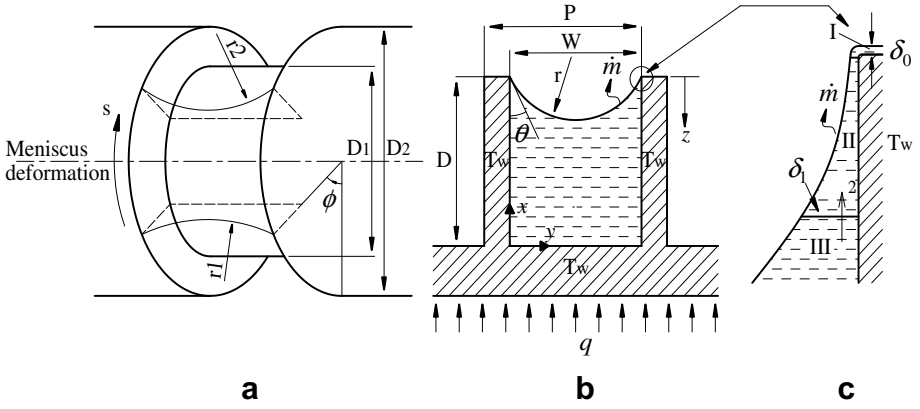

Fig. 3. The schematic of capillary-assisted evaporation along a circumferential rectangular micro-groove and the extended meniscus: (a) the rectangular micro-groove, (b) ϕ-directional cross-section, and (c) the extended meniscus.

For rectangular micro-grooves, if the axial distance exceeds some value, a "saturation jump" may appear and the "corner flow" may occur afterwards. In the situation of "corner flow", the axial liquid flow rate becomes very small, therefore the maximum heat flux supported by the groove decreases sharply which is unfavorable. Based on the research in the literature [20], a micro trapezoidal groove with the bottom width of 0.1 mm and the length of 10 mm, a maximum heat flux of 0.25 MW/m^2 can be supported. Therefore, for the normal geometry of the micro-grooves and working conditions applied in the evaporators inside refrigeration and air-conditioning machines, the appearance of "corner flow" can be excluded. In this paper, the crossing point between the evaporating thin film region and the non-evaporating adsorbed film region is always assumed to coincide with the apex of the groove. Also, the temperature of the groove's wall is assumed uniform for the high thermal conductivity of pure copper and small groove depth.

4. Experimental investigation

4.1. Experimental setup

The schematic diagram of the experimental setup is shown in Fig. 4. The test system takes the form of gravity heat pipe. The tested tube with enhanced outside surface of circumferential micro rectangular grooves is located at the center of a cylindrical evaporator. The heating fluid flows inside the tube to discharge the heat needed by evaporation. The vapor of the working fluid produced flows upwards to a coil condenser and is condensed by the cooling fluid inside the coil. The condensate returns to the evaporator by gravitation force through a glass tube level meter. A vacuum diaphragm valve is installed after the level meter that can cut off the condensate flowing back to the evaporator. Therefore, the lower part of the setup can be thought to be a single tube evaporator and the tested tube can be altered easily. The heating fluid and cooling fluid are supplied by two thermostats, respectively. The temperatures of heating fluid inlet, outlet and cooling fluid inlet, outlet are measured by four-wire Pt100 temperature sensors. The outside wall temperature of the tested tube are measured by 9 T-type thermocouples which are arranged at the tube's inlet, middle and outlet axial cross-sections, respectively, i.e., three for each cross-section and 120° between two thermocouples. All temperature sensors are calibrated by the standard mercury temperature meter with a measurement uncertainty of ±0.05 °C. The arithmetic mean value of these nine thermocouples is thought to be the wall temperature. The evaporating pressure is measured by an absolute pressure transducer with a measurement range of 0–20,000 Pa and a measurement uncertainty of ±40 Pa. The flow rates of heating and cooling fluids are measured by flow meters with measurement accuracy of ±1.0%.

4.2. Experimental scheme

The liquid–vapor interface curvature K increases gradually as the liquid flows along the tube's axial direction. When the immersion depth of the tested tube in the liquid decreases, the groove's axial distance from the liquid inlet to the tube's top outside surface increases. Therefore the curvature K can reach a bigger value that means a bigger axial mean curvature. Big curvature means big mass

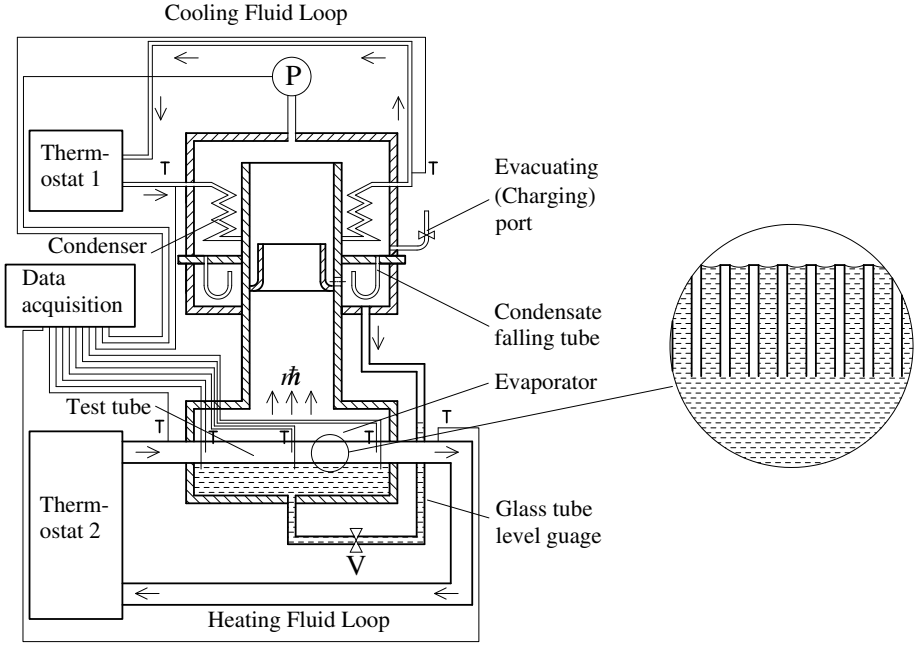

Fig. 4. The schematic of experimental setup: P, pressure gauge; T, temperature sensor; V, valve.

transfer area and thinner liquid film in the intrinsic meniscus region, thus big evaporating mass flow rate.

The dimensionless liquid level γ can be introduced, which is defined as the ratio of the immersion depth to the tube's outer diameter. In this experiment, the influence of γ on the evaporation heat transfer coefficient will be investigated. The values of γ of 1/4, 1/2, 3/4, and 1 are involved in the experiment.

Under the fixed evaporating pressure, the change of the superheating temperature of the groove's wall will change the heat flux transferred and the liquid temperature. Therefore, the thermophysical parameters of the liquid will be changed, which will change many important parameters such as the liquid–vapor interface curvature, the film thickness in the intrinsic meniscus region and evaporating thin film region, the z-direction length that the later region spans, etc. Under the fixed superheating temperature, the change of the evaporating pressure will bring the similar effect.

In the experiment, the superheating temperatures of 1.0–5.0 °C under the evaporating saturated temperature of 5.0 and 15.0 °C are investigated, respectively. The evaporation saturated temperature of 5.0 °C is usually adopted by standard water chillers; and those of 15.0 °C has the potential of being applied in the air-conditioning systems using dry fan coils in which cooling and dehumidification have been treated independently. The evaporating saturated temperature of 5.0–15.0 °C are involved under the superheating temperature of 3.0 °C. In the experiment, the temperature decrease of the heating fluid flowing inside the tested tube is controlled to be within 0.1 °C by adjusting the flow rate.

Four types of enhanced heat transfer tubes with the structure parameters listed in Table 1 are tested in the experiment. Water is chosen as the evaporating liquid. The tested working conditions are listed in Table 2.

4.3. Results and discussion

The ratio of the groove's depth to its width $\Lambda = D/W$ is introduced that indicates the similar extent of the groove to the space between two parallel and infinite plain plates. Then the four tested tubes (1#–4#) are labeled with $\Lambda = 5.0,2.5,2.0,1.0$, respectively. The total heat flux of the tested tube, Q can be calculated by

$$Q = \rho \frac{\pi d^2}{4} \Delta H h_{fg} / \Delta t, \tag{2}$$

Table 1
Structural parameters of the heat transfer tubes tested

No.	D_1 (mm)	D (mm)	W (mm)	P (mm)	L (mm)	Axial cross-section
1#	18	1.0	0.2	0.35	360	Rectangular
2#	18	0.5	0.2	0.35	360	Rectangular
3#	18	1.0	0.5	0.65	360	Rectangular
4#	18	0.5	0.5	0.65	360	Rectangular

Note: The tube material is pure copper.

Table 2
The working conditions involved in the experiment

T_e	γ							
	1/4	1/2					3/4	1
	ΔT (°C)							
	4	1	2	3	4	5	4	4
5	X	X	X	X	X	X	X	X
7	0	0	0	X	0	0	0	0
9	0	0	0	X	0	0	0	0
11	0	0	0	X	0	0	0	0
13	0	0	0	X	0	0	0	0
15	X	X	X	X	X	X	X	X

Note: X, included; 0, excluded.

where ΔH is the liquid level change inside the glass tube level meter within the time interval Δt and h_{fg} is the latent heat of evaporation of water. The capillary-assisted evaporation heat transfer coefficient is given as

$$h = \frac{Q}{A\Delta T}, \tag{3}$$

where A is the heat transfer area based on the groove bottom diameter, i.e., $A = \pi D_1^2 L/4$, ΔT is the temperature difference between the tube wall temperature (assumed uniform) and the saturated temperature corresponding to the evaporation pressure.

4.3.1. The effect of the dimensionless liquid level γ

In the experiment, the tested tube is partly immersed into the liquid. For the part of the tube's outside surface under the free liquid surface, the heat transfer with small superheating temperature (<5.0 °C) is characterized by natural convection that is very weak. Also, the micro-grooves have no enhancement effect on the natural convection heat transfer; for the part of the tube's outside surface over the free liquid surface, the heat transfer is characterized by thin film evaporation which has a high efficiency. Therefore, a smaller γ will lead to a higher h. A quantitative relation between h and γ is given in Fig. 5. As shown in the figure, for $\gamma = 1/4$, $T_e = 5.0 \pm 0.1$ °C, $\Delta T = 4.0 \pm 0.1$ °C and $\Lambda = 5.0$, the evaporation heat transfer coefficient h can reach 5500 W/m^2 K. With higher T_e, a higher h can be obtained.

4.3.2. The effect of superheating temperature

The influences of superheating ΔT on the capillary-assisted evaporation heat transfer coefficient h, with the evaporating saturated temperatures $T_e = 5.0 \pm 0.1$ and 15.0 ± 0.1 °C are given in Fig. 6. The experimental results have indicated a decrease of h with ΔT increasing under the same T_e and γ. When the superheating temperature changes from 5.0 to 1.0 °C, an increase of 30–60% of the evaporation heat transfer coefficient can be obtained. Increasing superheating temperature will decrease the ratio of the heat flux across the evaporating thin film region to the total heat flux, therefore the evaporation heat transfer

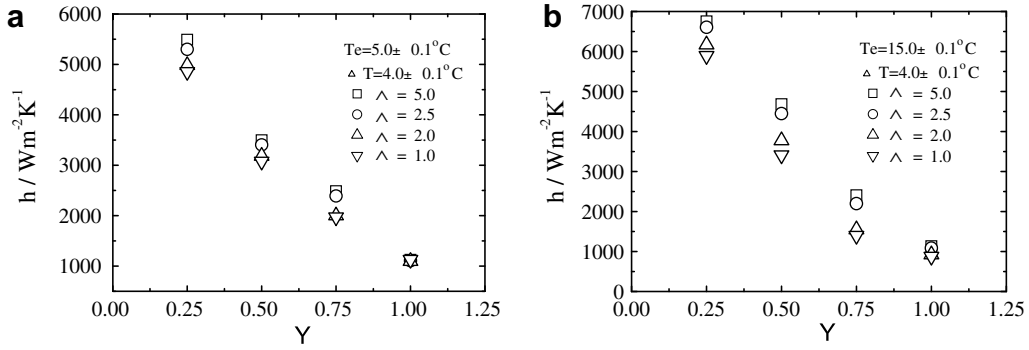

Fig. 5. Variation of the capillary-assisted evaporation heat transfer coefficient h with the dimensionless liquid level γ: (a) $T_e = 5$ °C and (b) $T_e = 15$ °C.

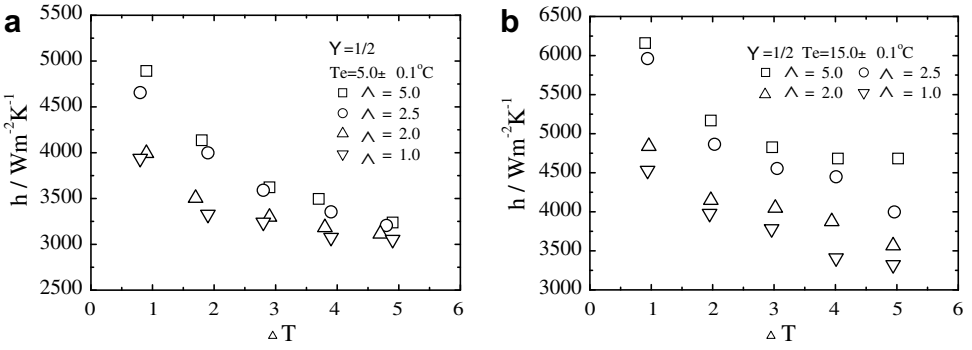

Fig. 6. Variation of the capillary-assisted evaporation heat transfer coefficient h with the superheating temperature ΔT: (a) $T_e = 5$ °C and (b) $T_e = 15$ °C.

coefficient h will be reduced. From the experimental results, we can also draw a conclusion that the heat transfer efficient in the evaporation thin film region is higher in comparison with that in the intrinsic meniscus region.

4.3.3. The effect of evaporating pressure

When the evaporating pressure increases, under the same superheating temperature, the liquid temperature will increase which will lead to the increase of liquid thermal conductivity and the decrease of the kinetic viscosity, and surface tension. Therefore, the increase of evaporating pressure can bring two benefits: one is the increase of the evaporation mass flux across the curved liquid–vapor interface; the other is the increase of the liquid flow rate in the evaporation thin film region. So, the evaporation heat transfer coefficient h will increase with the evaporating pressure, as can be proved by the experimental results given in Fig. 7. Under the superheating temperature of 3.0 ± 0.1 °C and dimensionless liquid level of 1/2, an increase of 15–30% of h can be obtained when the evaporating saturated temperature increases from 5.0 to 15.0 °C. In addition, for the tube with higher Λ, the increase of h is more evident.

4.3.4. The effect of shape parameter Λ

The groove's shape parameter Λ, i.e., the ratio of the groove's depth to the width, indicates the similar extent of the groove to a space between two parallel finite plain plates. From Figs. 5–7, it is evident that a bigger Λ is beneficial for the capillary-assisted evaporation. Given the groove's bottom diameter D_1 of 18 mm, the evaporation heat transfer coefficient h increases slowly when $\Lambda < 2.0$ and becomes fast afterwards. However, when the value of Λ exceeds 2.5, the increase of h becomes slowly again. Thus, considering the fabrication difficulty and cost, the value of Λ 2.5 is preferred.

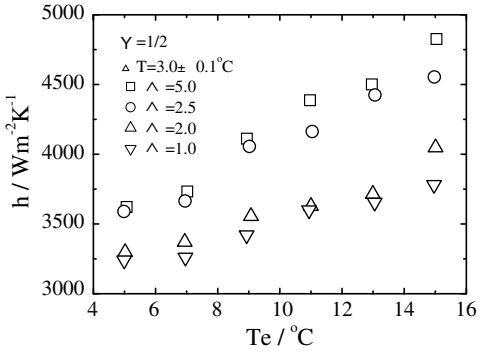

Fig. 7. Variation of the capillary-assisted evaporation heat transfer coefficient h with the evaporation saturated temperature T_e.

5. Error analyses

According to the error transfer theory, the error of the capillary-assisted evaporation heat transfer coefficient h can be determined, based on Eq. (3), by

$$\frac{\Delta(h)}{h} = \frac{1}{A\Delta T}\frac{\Delta(Q)}{h} - \frac{Q}{A}\frac{1}{(\Delta T)^2}\frac{\Delta(\Delta T)}{h} = \frac{\Delta(Q)}{Q} - \frac{\Delta(\Delta T)}{\Delta T}, \quad (4)$$

where $\Delta(Q)/Q$ can be calculated, based on Eq. (2), by

$$\frac{\Delta(Q)}{Q} = \frac{\Delta(\Delta H)}{\Delta H} - \frac{\Delta(\Delta t)}{\Delta t}. \quad (5)$$

Therefore, the relative error of h can be obtained by substituting Eq. (5) into (4)

$$\frac{\Delta(h)}{h} = \frac{\Delta(\Delta H)}{\Delta H} - \frac{\Delta(\Delta t)}{\Delta t} - \frac{\Delta(\Delta T)}{\Delta T}, \quad (6)$$

where the liquid level change ΔH inside the glass tube level meter has a maximum error of 1 mm, Δt is measured by time meter and the maximum error can be controlled to be within 2 s, the maximum error of the superheating temperature ΔT is within ± 0.1 °C. In the experiment, the time interval Δt is chosen as 300 s, the smallest values of ΔT and ΔH in the experiment are 1 °C and 106 mm, respectively. Hence, the maximum relative error of h is 11.6%.

6. Comparison to falling film evaporation

Falling film evaporation heat transfer is widely applied for the working fluids with low saturated vapor pressure. In such case, a closed circulating pump and liquid spray equipment are needed for the liquid distribution on the outside surfaces of heat transfer tubes. Comparing to falling film evaporation, the capillary-assisted evaporation have two advantages: one is no need of the circulating pump and liquid spray equipment; the other is the equality of liquid distribution on the outside surface of heat transfer tubes. Therefore, the evaporator applying capillary-assisted evaporation heat transfer is simple and reliable. Under the dimensionless liquid level $\gamma = 1/2$, evaporating temperature $T_e = 5.0 \pm 0.1$ °C and superheating temperature $\Delta T = 4.0 \pm 0.1$ °C, the capillary-assisted evaporation heat transfer coefficient h can reach 3100–3500 W/m^2 K. According to the literature [1], in LiBr–water absorption machines, with the evaporating temperature $T_e = 5.0$ °C, the chilled water inlet temperature of 12 °C and outlet temperature of 7 °C, the falling film evaporation heat transfer coefficient is usually 2800–4500 W/m^2 K. Though the heat transfer coefficient of capillary-assisted evaporation is slightly lower than that of falling film evaporation, the simple structure and higher reliability as well as lower cost make capillary-assisted evaporators have the potential to be applied widely. The use of capillary-assisted evaporators in the silica gel–water adsorption chiller developed by the research team of SJTU is a good example [21].

7. Conclusions

This paper introduces the micro-scale capillary-assisted evaporation heat transfer into normal-scale applications. The heat transfer tubes used in capillary-assisted evaporators have enhanced outside surfaces with circumferential micro-grooves which can realize equally liquid distribution through capillary suction. Such evaporators possess many advantages such as structural simplicity, high reliability, high heat transfer efficiency, low cost, etc.

This paper has carried out the quantitative investigation of the dependence of the capillary-assisted evaporation heat transfer coefficients on the micro-grooves' geometries and working conditions. A single-tube capillary-assisted evaporator has been designed and experimentally investigated. The following conclusions can be obtained through the experiment:

1. The capillary-assisted evaporation heat transfer coefficient has a positive relation with the evaporating pressure and negative relations with the liquid level and superheating temperature.
2. According to the experimental results achieved under refrigeration and air conditioning working conditions, with the dimensionless liquid level $\gamma = 1/2$, the capillary-assisted evaporation can get a heat transfer coefficient close to that of the falling film evaporator in LiBr–water absorption machines.
3. Considering both the heat transfer efficiency and cost, there exists an optimal value for the micro-groove's shape parameter Λ, $\Lambda = 2.5$ is preferred based on the investigations of this research.

Acknowledgements

This work was supported by the National 863 Program (Hi-Tech Research and Development Program of China) under the contract No. 2006AA05Z413.

References

[1] Y.Q. Dai, Y.Q. Zheng, LiBr–water Absorption Machine, first ed., Chinese National Defence Industry Press, Beijing, China, 1980.
[2] G.P. Peterson, H.B. Ma, Theoretical analysis of the maximum heat transport in triangular grooves: a study of idealized micro heat pipes, ASME J. Heat Transfer 118 (1996) 731–739.
[3] J.M. Ha, G.P. Peterson, The interline heat transfer of evaporating thin films along a micro grooved surface, ASME J. Heat Transfer 118 (1996) 747–755.
[4] Jinliang Wang, Ivan Catton, Enhanced evaporation heat transfer in triangular grooves covered with a thin fine porous layer, Appl. Therm. Eng. 21 (2001) 1721–1737.
[5] A. Sivaraman, S. De, S. Dasgupta, Experimental and theoretical study of axial dryout point for evaporation from V-shaped microgrooves, Int. J. Heat Mass Transfer 45 (2002) 1535–1543.
[6] I. Catton, G.R. Stroes, A semi-analytical model to predict the capillary limit of heated inclined triangular capillary grooves, ASME J. Heat Transfer 124 (2002) 162–168.
[7] S.S. Panchamgam, S.J. Gokhale, J.L. Plawsky, Experimental determination of the effect of disjoining pressure on shear in the contact line region of a moving evaporating thin film, ASME J. Heat Transfer 127 (2005) 231–243.
[8] Jeong-Se Suh, Ralph Greif, Costas P. Grigolopoulos, Friction in micro-channel flows of a liquid and vapor in trapezoidal and sinusoidal grooves, Int. J. Heat Mass Transfer 44 (2001) 3103–3109.

[9] S.S. Panchamgam, J.L. Plawsky, P.C. Wayner Jr., Microscale heat transfer in an evaporating moving extended meniscus, Exp. Therm. Fluid Sci. 30 (8) (2006) 745–754.
[10] Kyoungwoo Park, Kwan-Soo Lee, Flow and heat transfer characteristics of the evaporating extended meniscus in a micro-capillary channel, Int. J. Heat Mass Transfer 46 (2003) 4587–4594.
[11] Wei Qu, Tongze Ma, Jianyin Miao, Jinliang Wang, Effects of radius and heat transfer on the profile of evaporating thin liquid film and meniscus in capillary tubes, Int. J. Heat Mass Transfer 45 (2002) 1879–1887.
[12] S.W. Tchikanda, R.H. Nilson, S.K. Griffiths, Modeling of pressure and shear-driven flows in open rectangular microchannels, Int. J. Heat Mass Transfer 47 (2004) 527–538.
[13] R.H. Nilson, S.W. Tchikanda, S.K. Griffiths, M.J. Martinez, Steady evaporating flow in rectangular microchannels, Int. J. Heat Mass Transfer 49 (2006) 1603–1618.
[14] D.C. Wang, Z.Z. Xia, J.Y. Wu, R.Z. Wang, H. Zhai, W.D. Dou, Study of a novel silica gel–water adsorption chiller. Part I. Design and performance prediction, Int. J. Refrig. 28 (7) (2005) 1073–1083.
[15] H.M. Sabir, A.C. Bwalya, Experimental study of capillary-assisted water evaporators for vapour-absorption systems, Appl. Energy 71 (2002) 45–57.
[16] H. Honda, Y.S. Wang, Theoretical study of evaporation heat transfer in horizontal microfin tubes: stratified flow model, Int. J. Heat Mass Transfer 47 (2004) 3971–3983.
[17] A. Faghri, Heat Pipe Science and Technology, Taylor & Francis, New York, NY, 1995.
[18] R.Z. Wang, J.Y. Wu, Y.J. Dai, W. Wang, Z.S. Jiang, Adsorption Refrigeration, Publishing House of Mechanical Industry, Beijing, China, 2002.
[19] J.A. Schonberg, S. DasGupta, P.C. Wayner Jr., An argumented Young–Laplace model of an evaporating meniscus in a microchannel with high heat flux, Exp. Therm. Fluid Sci. 10 (1995) 163–170.
[20] Takashiro Tsukamoto, Ryoji Imai, Thermal characteristics of a high heat flux micro-evaporator, Exp. Therm. Fluid Sci. 30 (2006) 837–842.
[21] R.Z. Wang, Efficient adsorption refrigerators integrated with heat pipes, Appl. Therm. Eng. 28 (2008) 317–326.